Studies of pure and nitrogen-incorporated hydrogenated amorphous carbon thin films and their possible application for amorphous silicon solar cells

Neeraj Dwivedi, Sushil Kumar, and Hitendra K. Malik

Articles you may be interested in

Photoconductivity and characterization of nitrogen incorporated hydrogenated amorphous carbon thin films
J. Appl. Phys. **112**, 113706 (2012); 10.1063/1.4768286

Application of amorphous carbon based materials as antireflective coatings on crystalline silicon solar cells
J. Appl. Phys. **110**, 043510 (2011); 10.1063/1.3622515

Superlow friction of titanium/silicon codoped hydrogenated amorphous carbon film in the ambient air
J. Appl. Phys. **108**, 033510 (2010); 10.1063/1.3462469

Polymeric amorphous carbon as p-type window within amorphous silicon solar cells
Appl. Phys. Lett. **82**, 3979 (2003); 10.1063/1.1580636

Effects of deposition temperature on the properties of hydrogenated tetrahedral amorphous carbon
J. Appl. Phys. **82**, 4566 (1997); 10.1063/1.366193

Studies of pure and nitrogen-incorporated hydrogenated amorphous carbon thin films and their possible application for amorphous silicon solar cells

Neeraj Dwivedi,[1,2] Sushil Kumar,[1,a)] and Hitendra K. Malik[2]

[1]*Physics of Energy Harvesting Division, National Physical Laboratory (CSIR), K.S. Krishnan Road, New Delhi 110012, India*
[2]*Department of Physics, Indian Institute of Technology Delhi, New Delhi 110016, India*

Hydrogenated amorphous carbon (a-C:H) and nitrogen-incorporated a-C:H (a-C:N:H) thin films were deposited using radio frequency–plasma-enhanced chemical vapor deposition technique and studied for their electrical, optical, and nano-mechanical properties. Introduction of nitrogen and increase of self bias enhanced the conductivity of a-C:H and a-C:N:H films, whereas current-voltage measurement reveals heterojunction formation due to their rectifying behavior. The bandgap of these films was changed over wide range from 1.9 eV to 3.45 eV by varying self bias and the nitrogen incorporation. Further, activation energy was correlated with the electronic structure of a-C:H and a-C:N:H films, and conductivity was discussed as a function of bandgap. Moreover, a-C:N:H films exhibited high hardness and elastic modulus, with maximum values as 42 GPa and 430 GPa, respectively, at −100 V. Observed fascinating electrical, optical, and nano-mechanical properties made it a material of great utility in the development of optoelectronic devices, such as solar cells. In addition, we also performed simulation study for an a-Si:H solar cell, considering a-C:H and C:N:H as window layers, and compared their performance with the a-Si:H solar cell having a-SiC:H as window layer. We also proposed several structures for the development of a near full-spectrum solar cell. Moreover, due to high hardness, a-C:N:H films can be used as a protective and encapsulate layer on solar cells, especially in n-i-p configuration on metal substrate. Nevertheless, a-C:H and a-C:N:H as a window layer can avoid the use of additional hard and protective coating and, hence, minimize the cost of the product. © *2012 American Institute of Physics*. [doi:10.1063/1.3675164]

I. INTRODUCTION

Among various possible sources, the solar energy is found to be the best alternative for non-conventional energy. Solar cell is a p-n junction device that converts solar energy into electrical energy by photovoltaic effect. The commonly used structures for solar cells are either p-n junction or p-i-n junction, whereas the most broadly used material for solar cell is crystalline silicon that uses p-n junction-type structure to convert solar energy into electrical energy. Extensive research on crystalline silicon solar cells has been performed. However, crystalline silicon–based solar cells are quite costly, as they use thick silicon wafers, which cover ∼ 65% cost of fabricated solar cells. Moreover, crystalline silicon has fixed small bandgap of 1.1 eV that may lead to more absorption losses. In contrast, solar cells made up of thin film materials are quite cheaper and have feasibility to tune its bandgap over a wide range. Thus, by tuning the bandgap, one can cover the large solar spectrum that will result in enhanced efficiency. So, presently, thin film solar cells are found to be a subject of great importance.[1] Thin film solar cells generally involve either p-i-n or n-i-p type structure to convert solar energy into electrical energy. In thin film–based solar cells, the p-layer generally acts as a window layer and possesses high bandgap, the i-layer acts as an absorber layer, and the n-layer acts as a collector layer. Almost full incoming light absorb in the i-layer, resulting in the creation of electron-holes pairs, which are further separated by junction field. The minority carriers in the depletion region, such as electrons, are then moved toward the n-layer and holes are moved toward the p-layer and become majority carrier. This way, a photo current flows into the device and conversion of solar energy into electrical energy takes place. The hydrogenated amorphous silicon (a-Si:H) is found to be the most widely used material for the generation of thin film solar cells. However, there are certain limitations with a-Si:H as window layer, some of which are mentioned below:

(a) Light-induced degradation (Stabler-Wronski effect)
(b) Highly flammable, toxic, and corrosive gases, such as silane (SiH_4), phosphine (PH_3), and diborane (B_2H_6), are used for deposition of a-Si:H-based p-i-n solar cells
(c) The third and most important issue with a-Si:H-based solar cells is its lower bandgap (∼1.7 eV)

Palit and Chatterjee[2] and Rath and Schropp[3] suggested microcrystalline (μc)-a-Si:H as the p-layer for improving the efficiency and resolving the light-induced degradation problem. However, in order to realize μc-a-Si:H as the p-layer, its deposition on transparent conducting oxide (TCO) is found to be quite complex. Actually, during the growth of μc-a-Si:H, the hydrogen plasma intensity must be high. On the other hand, under the high hydrogen plasma intensity condition, the surface of the TCO may damage, which results in poor electronic contact between the p-layer and the TCO.

a)Electronic mail: skumar@nplindia.org. Fax: +91-11-45609310.

     111, 014908-1

Moreover, μc-a-Si:H has low bandgap; hence, it may also introduce significant heat losses. As mentioned, the bandgap of a-Si:H is just $\sim$1.7 eV, which can be tuned up to $\sim$ 2-2.1 eV by carbon doping.[4,5] Thus, a fabricated a-SiC:H alloy can act as an excellent p-layer and may reduce the Stabler-Wronski effect. However, a-SiC:H as the p-layer also has certain limitations, such as band offset, proper stoichiometry between Si and C, bandgap controlling, and small bandgap variation. Moreover, with such an alloy, the creation of tandem and multijunction solar cells is quite difficult. Thus, there is great demand to search such a material, whose bandgap could vary over a wide range and, therefore, may offer the development of efficient tandem (multijunction) solar cells.

In this regard, hydrogenated amorphous carbon (a-C:H), which is quite analogous to a-Si:H, was found to be an appropriate material, due to its bandgap feasibility over a wide range. Thus, by using different bandgap layers of a-C:H, one may construct a-C:H-based tandem solar cells. A series of reports pertaining to development of a-C:H-based solar cells can be found in the literature.[6–8] The a-C:H and nitrogen-incorporated a-C:H (a-C:N:H) thin films may also be employed for generation of heterojunction solar cells. Recently, we[9,10] have made an n-type a-C:H/p-type Si heterojunction diode as well as improved the electronic properties of DLC by introduction of metal dots. Tinchev et al.[11] discussed the role of bandgap in an a-C:H-based solar cell. In addition to bandgap feasibility, a-C:H films also exhibit higher transmission. Thus, because of this property, the a-C:H-based thin layer can also be used as a window layer in a-Si:H-based solar cells. Another important issue with solar cells is their stability under exposure of high energy radiation, as their efficiency falls down under this situation. Space vehicles, in which solar cells are embedded, see high energy radiation, including Gamma radiation and solar wind. The a-Si:H-based and other most important solar cells are quite soft, and their efficiency may degrade under exposure of such a high energy radiation.[12] Hence, an additional hard and protective over layer is used to avoid degradation problem in these cells. Due to their excellent mechanical properties, a-C:H and a-C:N:H films can also be used as a hard and protective layer on solar cells. However, such additional layers enhance the cost of cells. Thus, by employing a-C:H and a-C:N:H as the window layer, the stability problem of soft solar cells gets solved without any need of an additional protective layer.

However, in order to explore a-C:H as a material for solar cell application, one has to solve certain issues. The most important issue with a-C:H is its high residual stress that leads to detachment of the film from the substrate. Many authors have proposed a nitrogen-incorporated a-C:H (a-C:N:H) film to minimize its residual stress. We have reduced the stress and improved the nano-mechanical properties of DLC by some modification.[13–17] Another important issue with a-C:H is its lower mobility and, therefore, lower conductivity. Such an issue can also be addressed by nitrogen incorporation in a-C:H (a-C:N:H). In addition, due to complex structure, understanding of electrical transport was also found to be a subject of discussion. The third issue is its lower

absorbance in the visible region. Nonetheless, lower absorbance is good for employing them as a window layer, but bad for employing them as an absorber i-layer in solar cells.

Therefore, in the present work, we report the growth of a-C:H and a-C:N:H films under varied self biases and their characterizations for electronic, optical and nano-mechanical properties. The aim of the present study is to explore a-C:H and a-C:N:H as a material for solar cell application. The theoretical a-Si:H thin film solar cell, considering a-C:H and a-C:N:H as the window layer, was prepared and their performance compared with an a-SiC:H window layer–contained solar cell. In addition, some basic characterizations, such as TOF-SIMS and FTIR for composition and bonding environment, respectively, and SEM for surface morphology, are also performed. We also tried to resolve various issues of a-C:H and a-C:N:H films.

II. EXPERIMENTAL DETAILS

Two sets of a-C:H and a-C:N:H thin films were deposited using asymmetric, capacitive-coupled RF-PECVD technique at base pressure better than 10^{-5} Torr. In the first set, five a-C:N:H films were grown on well-cleaned p-type Si $\langle 100 \rangle$, corning 7059 glass, ITO, and stainless steel substrates under varying self biases from -25 to -400 V, whereas, in the second set, three a-C:H films were deposited on well-cleaned n-type Si $\langle 100 \rangle$, corning 7059 glass, ITO, and stainless steel substrates under varying self biases from -30 to -180 V. The acetylene and nitrogen gas pressures and other parameters in all the depositions were kept constant in order to see the role of self bias on various properties of these films.

The thicknesses of a-C:H films were measured using Taylor-Hobson talystep instrument and found to be 110, 170, and 220 nm at -30, -100, and -180 V, respectively, whereas the thickness of a-C:N:H films deposited at -25, -100, -200, -300, and -400 V were found to be 250, 310, 340, 365, and 412 nm, respectively. Optical properties were measured by Schimadzu ultraviolet-visible (UV-VIS) 1601 spectrophotometer. Temperature-dependent conductivity measurements in the temperature range from room temperature to 473 K have been carried out using a Keithley 610 C solid-state electrometer. I-V measurements were performed using a Keithley Pico ammeter. The residual stress of a-C:H and a-C:N:H films deposited on a Si substrate was determined based on the change in radius of curvature of the substrate before and after deposition, using a 500TC temperature-controlled film stress measurement system (M/s FSM Frontier Semiconductor, USA) by the Stoney formula given by

$$\sigma = \frac{E_s d_s^2}{6(1 - \nu_s) d_f} \left(\frac{1}{R_f} - \frac{1}{R_0} \right). \tag{1}$$

In Eq. (1), E_s, ν_s, d_s, and d_f are Young's modulus, Poisson ratio, and thicknesses of the substrate and film, respectively, and R_0 and R_f are the radii of curvature of substrate before and after film deposition. IBIS nanoindentation (Fisher-Cripps laboratories Pvt. Limited, Australia), having a triangular pyramid diamond Berkovich indenter with normal

angle of 65.3° between the tip axis and the faces of the triangular pyramid and the curvature of 150 nm–200 nm at the tip, were used to study the nano-mechanical properties of a-C:N:H films.

The AFORS-HET-2.4.1 software was employed to simulate the different a-Si:H thin film solar cells, where a-C:H and a-C:N:H were considered as the window layer. This software is based on a one-dimensional equation that solves various equations, including Poisson's equation and the transport equation for electrons and holes. The simulation was performed by varying a-C:H and a-C:N:H window layer bandgaps from 1.8 eV to 3.45 eV. The open circuit voltage (V_{oc}), short circuit current (I_{sc}), fill factor (FF), and efficiency (η) were analyzed as a function of the window layer bandgap at different thicknesses (5 nm–20 nm). In addition, the simulation for a-Si:H solar cells by considering a-SiC:H as the window layer was also performed and obtained efficiency was compared with the previous one. The parameters used in the present simulation were taken from standard references[18–24] and are given in Table I.

III. RESULTS AND DISCUSSION

A. TOF-SIMS, SEM, and FTIR analyses

TOF-SIMS was employed to evaluate the elemental composition of film from bulk. A typical TOF-SIMS depth profile of an a-C:N:H film grown at −100 V is shown in Fig. 1(a), which clearly reveals the presence of C, H, and N. Ion implantation theory suggests that lighter ions diffuse deeper into the substrate, where they lose energy. In contrast, heavier ions lose their energy near the surface of the substrate and, hence, they diffuse just near the substrate surface. From the depth profile, we can clearly see that lighter hydrogen ions diffuse deeper into the substrate than carbon and nitrogen ions. In addition, the diffusion of carbon ions was also comparatively deeper than nitrogen ions, because nitrogen ions are slightly heavier than carbon ions. A typical SEM micrograph of an a-C:N:H film deposited at self bias of −100 V is shown in Fig. 1(b). This micrograph reveals the creation of spherical-shaped carbon nanostructure with diameter ∼120 to 130 nm. These spheres were uniformly distributed over the entire surface.

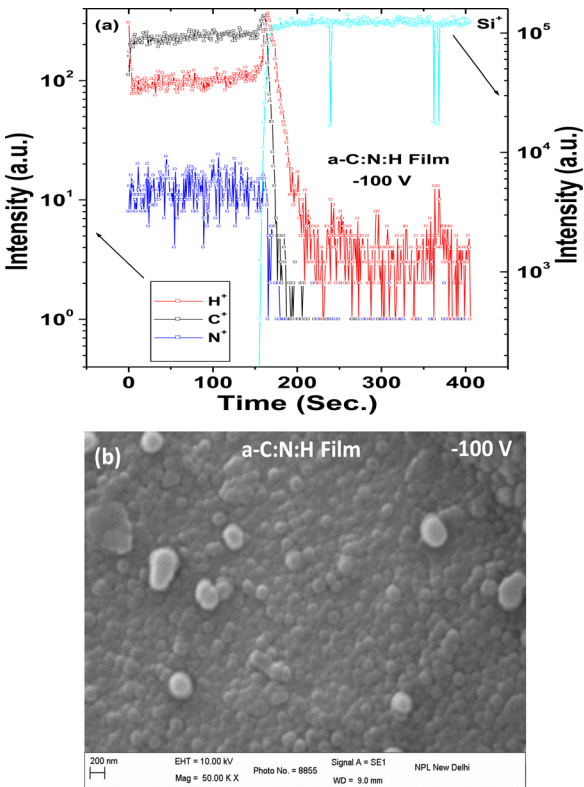FTIR analysis was performed to investigate the bonding environment of a-C:N:H films. Since C-H stretching

FIG. 1. (Color online) (a) Typical SIMS depth profile and (b) typical SEM picture of a-C:N:H film deposited at self bias of −100 V.

vibrations play a very important role in influencing the properties of a-C:H films, despite a-C:N:H films, the influence of bias on C-H stretching vibrations was also analyzed systematically. Several reports pertaining to estimation of sp^3 and sp^2 fractions of carbon by FTIR can be found in the literature, but it is still a subject of debate, because these fractions are based on C-H bonding. Nevertheless, hydrogen not only relaxes the stress and tunes the bandgap, but also stabilizes the diamond-like bonding.[25–27] Thus, the C-H based sp^3 and sp^2 fractions and their ratios are also very important to discuss and correlate with various properties of a-C:N:H films. The sp^3CH_n and sp^2CH_n bonding and sp^3/sp^2 ratios for various a-C:N:H films were estimated by deconvoluting the C-H stretching band, which is shown in Figs. 2(a)–2(d). The C-H-based sp^3 and sp^2 fractions and sp^3/sp^2 ratios were estimated by employing the following relations:

TABLE I. Input parameters used for simulation in the present study.

| Parameters	w-layer of a-SiC:H	w- layer of a-C:H/a-C:N:H	i-layer of a-Si:H	n-layer of a-Si:H
Relative permittivity (ε_r)	11.9	4.0	11.9	11.9
Electron mobility (μ_n, cm^2/V s)	5	0.001	5	5
Hole mobility (μ_p, cm^2/V s)	1	0.0001	1	1
Acceptor/donor 1×10^{19} (Concentration, cm^{-3})	1×10^{18}	1×10^{18}	…	
Band gap (eV)	1.8–2.5	1.8– 3.45	1.74	1.78
Electron affinity (eV)	3.9	2.0	3.9	3.9
Conduction band con. N$_C$, (cm^{-3})	1×10^{20}	1×10^{20}	1×10^{20}	1×10^{20}
Valence band con. N$_V$, (cm^{-3})	1×10^{20}	1×10^{20}	1×10^{20}	1×10^{20}
Thickness (nm)	5–20	5– 20	400	30
Density (g/cm^3)	2.328	2.4	2.328	2.328
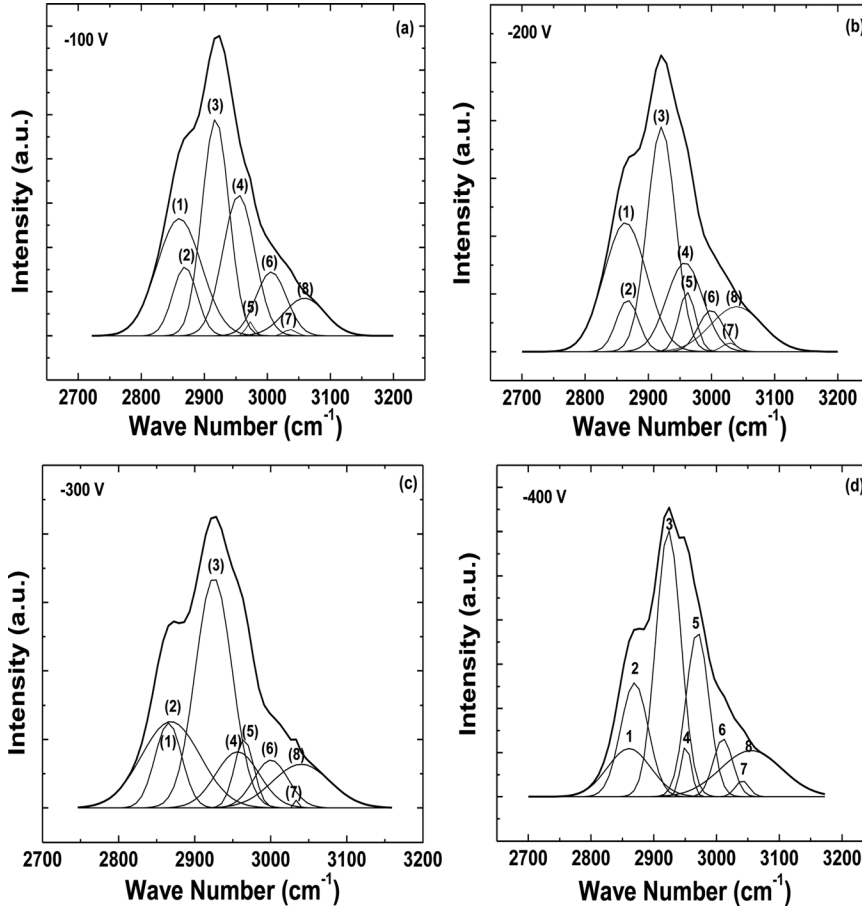
FIG. 2. Deconvoluted FTIR spectra in the range 2700 cm^{-1}−3200 cm^{-1} of a-C:N:H films deposited at self biases of (a) −100 V, (b) −200 V, (c) −300 V, and (d) −400 V.

$$\%sp^3 = \frac{\sum_{i=1}^{4} A_i}{\sum_{i=1}^{8} A_i} \times 100, \quad (2)$$

$$\%sp^2 = \frac{\sum_{i=5}^{8} A_i}{\sum_{i=1}^{8} A_i} \times 100, \quad (3)$$

where i = 1, 2, 3, 4, 5, 6, 7, and 8 and A_1, A_2, A_3, and A_4 are areas under the peaks for sp^{3}CH$_n$ bondings (peaks 1, 2, 3, and 4), whereas A_5, A_6, A_7, and A_8 are areas under the peaks for sp^{2}CH$_n$ bondings (peaks 5, 6, 7, and 8), respectively. The sp^3 fraction was found to decrease and sp^2 fraction to increase with the increasing of self bias from −100 V to −400 V. Due to combined effect, the sp^3/sp^2 ratio provides an actual bonding environment in the deposited films. Therefore, experimentally evaluated electrical and optical properties of a-C:N:H films were discussed in terms of the sp^3/sp^2 ratio. The variation of the sp^3/sp^2 ratio with self bias for different a-C:N:H films is depicted in Fig. 3. It is clear that the sp^3/sp^2 ratio varies inversely with the self bias. The maximum value of sp^3/sp^2 was observed as 4.6 at self bias −100 V, which was continuously decreased to 3.6, 3.3, and 1.6 at the self biases of −200 V, −300 V, and −400 V, respectively. Observed reduction in the sp^3/sp^2 ratio was due to the enhancement in graphite-like sp^2 bonding that is drastically increased beyond −300 V, leading to abrupt reduction in the sp^3/sp^2 ratio beyond −300 V.

B. Residual stress (S) of a-C:H and a-C:N:H films

Existence of a high level of residual stresses (S) in a-C:H films limits its wide spread industrial applications. Thus, there is a great interest to minimize S in a-C:H films without affecting their other properties. The variation of S with self bias of a-C:H and a-C:N:H films is shown in Fig. 4. It can be seen that, initially, with the increase of self bias from −30 to −100 V, the S of a-C:H films was increased from 2.1 GPa to 2.8 GPa. However, beyond −100 V, the S
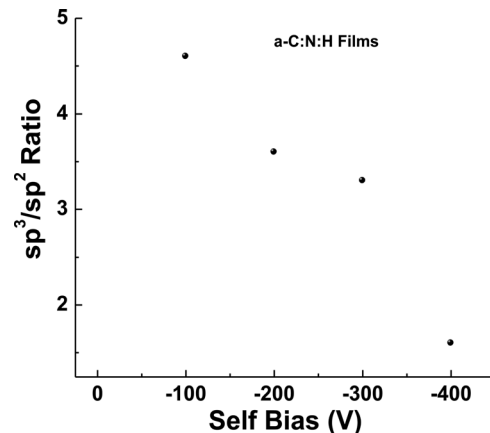

FIG. 3. Variation of sp^3/sp^2 with self bias for different a-C:N:H films.
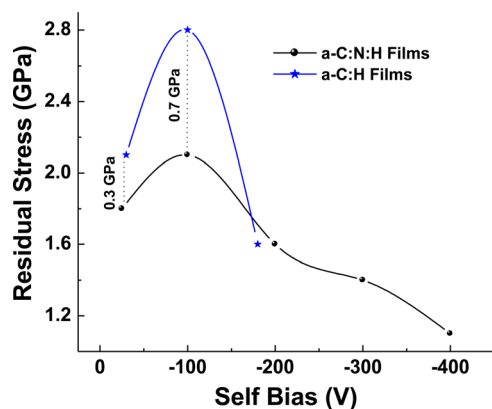
FIG. 4. (Color online) Variation of residual stress with self bias for different a-C:H and a-C:N:H films.

was decreased significantly and found to be 1.6 GPa at −180 V. Observed minimum S at a self bias of −180 V was due to initiation of graphite-like sp^2 bonding. On the other hand, the obtained maximum S at −100 V may be due to the reduction of the hydrogen fraction and increased diamond-like bonding. The film deposited at a low self bias of −30 V, although, possessed a high amount of hydrogen, but it also contained significant unbound hydrogen, resulting in S higher than film deposited at −180 V, but lower than film deposited at −100 V. The S in a-C:N:H films followed a similar trend and was found to be maximum at −100 V. The values of S in a-C:N:H films at self biases −25 V, −100 V, −200 V, −300 V, and −400 V were found to be 1.8 GPa, 2.1 GPa, 1.6 GPa, 1.4 GPa, and 1.1 GPa, respectively. Beyond −100 V, the observed decrease in S was due to the initiation of graphite-like sp^2 bonding that became dominant at higher self biases (−400 V). It is worth noting that the value of S in a-C:N:H films was significantly lower than a-C:H films, because nitrogen in a-C:N:H films (i) enhances the graphite-like sp^2 bonding, (ii) promotes sp^3 C–C debonding, and (iii) reduces the average coordination number.[13,28] Further, the S of a-C:N:H films was correlated with experimentally measured sp^3/sp^2 ratios. The S of an a-C:N:H film was varied in proportion with the sp^3/sp^2 ratio; that is, it decreased with the decreasing sp^3/sp^2 ratio.

C. Transmittance, absorbance, and optical bandgap analyses

In order to employ a-C:H and a-C:N:H films as window layers in solar cells, their transmittance must be very high for minimizing the recombination losses. On the other hand, in order to employ them as absorber layers, their absorption must be high, especially in the visible region, to generate a large number of electron-hole pairs. Figures 5(a) and 5(b) show the transmittance spectra of a-C:H and a-C:N:H films, respectively. The a-C:H films show less transmittance in UV, comparatively better in visible, and maximum in near IR regions. The transmittance of thin films strongly depends on the films' thickness, and an increase in self bias enhances the thickness of a-C:H films. Thus, the enhanced self bias reduces the transmittance of these films. Tinchev *et al.*[11] have also observed such an effect during their studies on
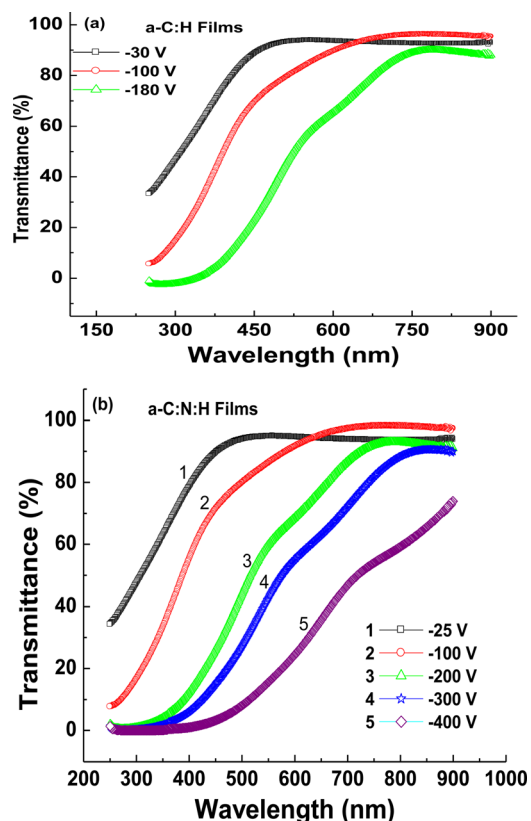

FIG. 5. (Color online) Transmittance spectra of different (a) a-C:H and (b) a-C:N:H films.

a-C:H films. It is important to mention that, up to ∼620 nm, the transmittance of the a-C:H film deposited at −30 V was found to be more than the film deposited at −100 V. However, beyond 620 nm, the reverse trend was observed, and the a-C:H film deposited at −100 V started to show more transmittance than film deposited at −30 V. This might be due to the fact that diamond exhibits very high optical transparency and, at −100 V, the maximum sp^3 bond and maximum diamond-like character a-C:H film may form. Observed transmittance in a-C:N:H films followed the similar trend and was found to decrease with the increasing self bias. Similar to a-C:H films, up to ∼650 nm, the transmittance of the a-C:N:H film deposited at −100 V was found to be lower than the film deposited at −25 V, but beyond ∼650 nm, the transmission of the film deposited at −100 V becomes more than the film deposited at −25 V. The reason for this may be the same as discussed in the previous case.

The absorbance spectra of a-C:H and a-C:N:H films are shown in Figs. 6(a) and 6(b), respectively. The absorbance also strongly depends on film thickness and varies linearly with it. The increase in self bias enhanced the absorbance in both types of the films due to an increase in the films' thickness. These films exhibited very higher absorbance in the UV region. It is worth noting that an increase in self bias not only enhances the absorbance, but also shifts it toward the visible region that can be seen from the absorbance spectrum of a-C:H films. The shifting of absorbance toward the visible region can be seen more clearly in a-C:N:H films, because, in this set of films, the self bias was varied from −25 V to −400 V. In addition, a-C:N:H films deposited at higher self
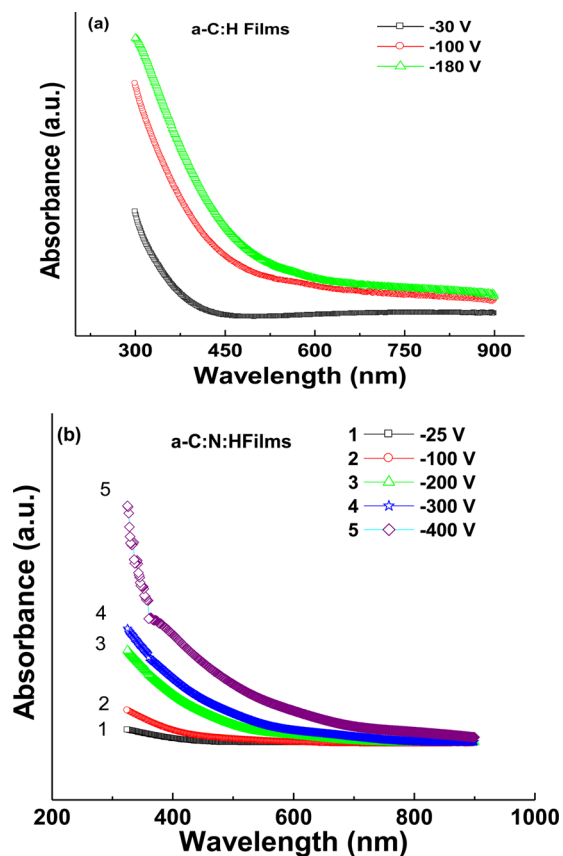
FIG. 6. (Color online) Absorbance spectra of different (a) a-C:H and (b) a-C:N:H films.

FIG. 7. (Color online) Variation of bandgap with self bias for different a-C:H and a-C:N:H films.

biases show more graphite-like sp^2 bonding and, therefore, may have higher conductivity. Thus, employing a-C:H and a-C:N:H films as an absorber i-layer, higher self biases should be preferred.

The optical bandgap (E_g) was found to be a main parameter while exploring a-C:H and a-C:N:H films as a material for photovoltaic application. In order to estimate bandgap of these a-C:H and a-C:N:H films, the absorption coefficient (α) was calculated using the relation $\alpha = [\ln\{(1 - R)/T\}]/d$, where R is the reflection, T is the transmission, and d is the thickness of the films. The bandgap of these films was estimated using Tauc plot $(\alpha h\nu)^{1/2}$ versus $h\nu$ curve by taking the asymptotic/tangent of the curve to the X axis.

The variation of bandgap versus self bias for a-C:H and a-C:N:H films is depicted in Fig. 7. In a-C:H films, initially, with increase in self bias from -30 V to -100 V, the bandgap was increased and attained maximum value, beyond which it dropped drastically. The values of bandgap at -30 V, -100 V, and -180 V were found to be 2.85 eV, 3.45 eV, and 2.7 eV, respectively. Observed bandgap values of a-C:N:H films followed the similar trend and initially increased with the increasing self bias from -25 V to -100 V and attained maximum value at -100 V, beyond which it decreased continuously. The values of bandgap in a-C:N:H films at -25 V, -100 V, -200 V, -300 V, and -400 V were found to be 2.75 eV, 3.33 eV, 2.42 eV, 2.32 eV, and 1.9 eV, respectively. On comparing the results of bandgap of a-C:H with a-C:N:H films, it was observed
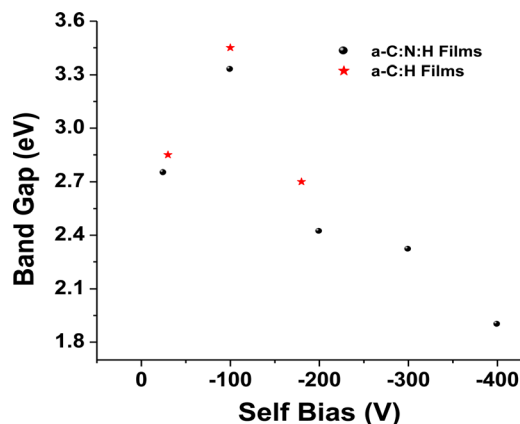
that addition of nitrogen in a-C:N:H films reduces the bandgap significantly. The bandgap in a-C:H and a-C:N:H films can be explained on the basis of a biphasic model, in which sp^2 clusters are embedded in an amorphous sp^3 matrix. These sp^2 clusters involve π-π* transition and control the bandgap of a-C:H films.[29] The addition of nitrogen in a-C:N:H films enhances the sp^2 clusters and narrows the π-π* transition, resulting in significant reduction in bandgap. Higher self bias also narrows the π-π* gap and minimizes the bandgap. The bandgap results are in good agreement with the sp^3/sp^2 ratio as well as stress results. It can be seen that the bandgap in a-C:H films was varied from 2.7 eV to 3.45 eV, whereas, in a-C:N:H films, it was varied from 1.9 eV to 3.33 eV. Overall bandgap in combined a-C:H and a-C:N:H films was varied from 1.9 eV to 3.45 eV. It is important to mention that, recently, we engineered the bandgap of a-C:H from 1.25 eV to 2.6 eV by oxygen plasma treatment.[30] Thus, by incorporating nitrogen, varying self bias, and doing some treatments, the deposition of tunable bandgap layers was made possible to be employed in the development of novel full-spectrum solar cells.

D. Conductivity analysis

Temperature-dependent conductivity measurements on a coplanar structure were performed on various a-C:H and a-C:N:H films under varied temperature from 300 K to 473 K. The variations of the inverse of temperature with conductivity of a-C:H and a-C:N:H films are depicted in Figs. 8(a)–8(h). The temperature-dependent conductivity in insulating to semiconducting films is given by

$$\sigma = \sigma_0 \exp(-\Delta E_A / kT),$$

where σ is the conductivity and σ_0 is the conductivity pre-exponential factors, ΔE_A is the activation energy, and k and T are the Boltzmann constant and temperature, respectively. The conductivity in both types of these films was found to increase with the increasing temperature, revealing their semiconducting behavior. Sharon et al.[31,32] have observed semiconducting behavior from camphor-pyrolyzed carbon films. Mukhopadhyay et al.[33] and Krishna et al.[34] have also observed semiconducting behavior, and they developed the
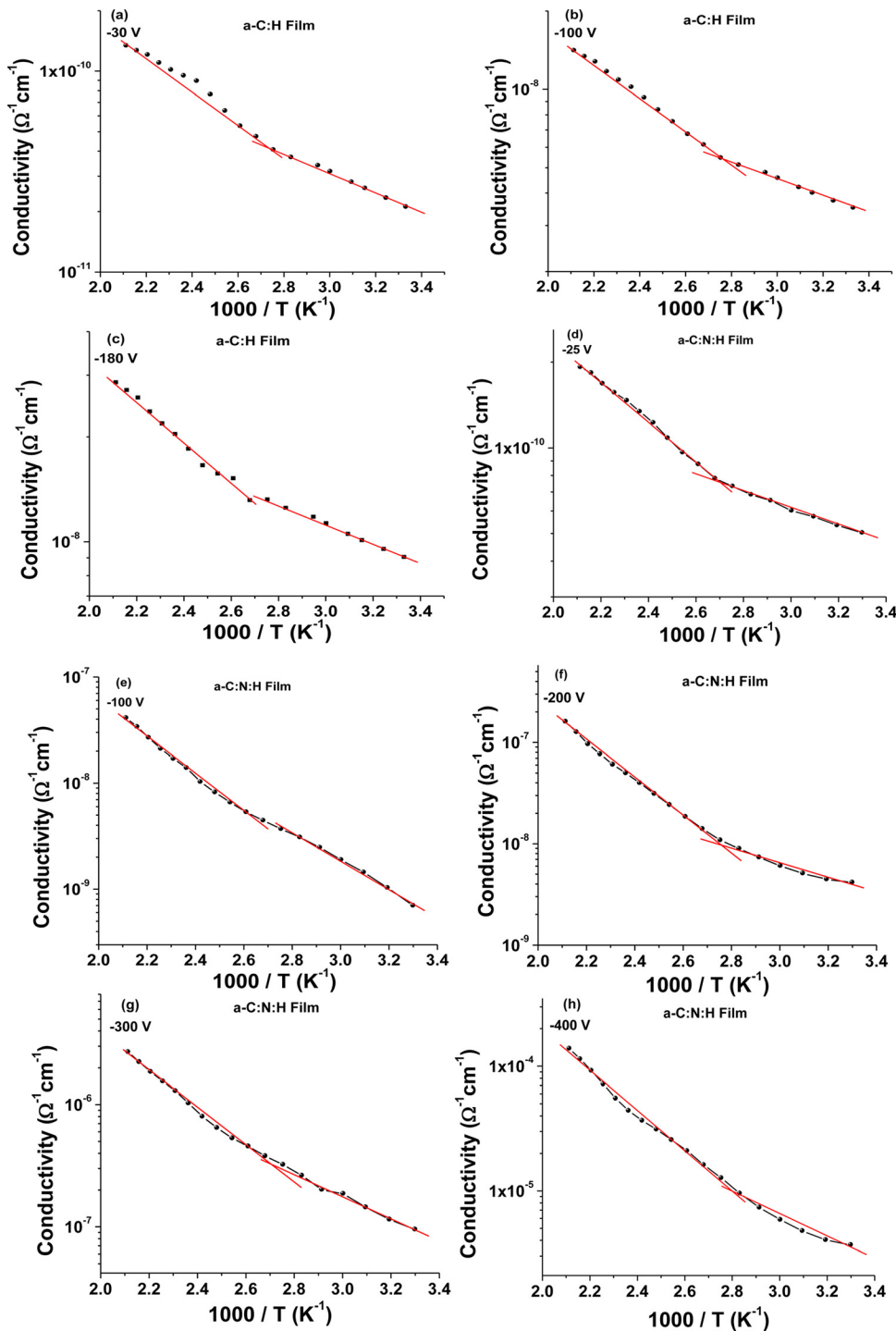
FIG. 8. (Color online) (a)-(h) Variation of conductivity with inverse of temperature for different a-C:H and a-C:N:H films.

photovoltaic cell from soot of camphor. Nevertheless, activation energy is an important electrical parameter, which suggests the possible conduction mechanism in the semiconductors. Activation energy (ΔE_A) in these films was estimated by the Arrhenius plot of conductivity versus the inverse of temperature, which is shown in Figs. 8(a)–8(h). It can be seen from Figs. 8(a)–8(h) that plots show two regimes: one in the lower temperature range (300 K–363 K) and the other in the higher temperature range (363 K–473 K). In this way, these films exhibited two modes of conduction with two activation energies and, hence, resultant conductivity is given by

$$\sigma = \sigma_{01} \exp(-\Delta E_{A1}/kT) + \sigma_{02} \exp(-\Delta E_{A2}/kT).$$

The first term, with activation energy E_{A1}, is dominant at a lower temperature range, whereas the second term, with activation energy E_{A2}, is dominant at a higher temperature range. The variation of activation energy (ΔE_{A1} and ΔE_{A2}) with self bias for a-C:H and a-C:N:H films is given in Fig. 9. The values of ΔE_{A1} were found to be lower than ΔE_{A2} in all a-C:H and a-C:N:H films, suggesting two different types of conduction. Actually activation energy is the amount of energy needed to lift the carrier from occupied states to unoccupied states. Hence, in ordered (crystalline) semiconductor, where a
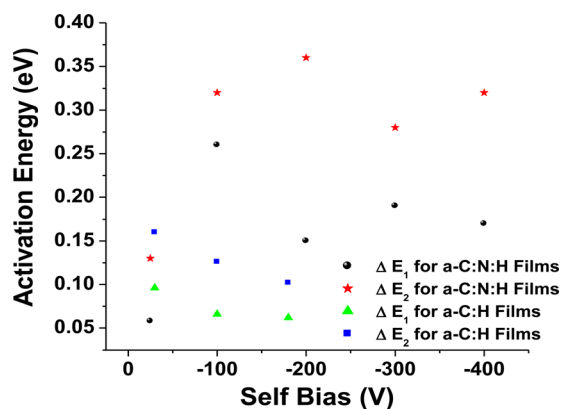
FIG. 9. (Color online) Variation of activation energy (ΔE_{A1} and ΔE_{A2}) with self bias for different a-C:H and a-C:N:H films.

forbidden gap lies between the Fermi level and conduction band, activation energy corresponds to the energy difference between the Fermi level and conduction band. However, in disorder semiconductors, this does not apply, strictly due to the difference in the electronic structure. Hence, activation energy in disorder semiconductors varies, depending upon the conduction type of the carriers. Based on the conduction mechanism in our samples and various other reports pertaining to this type of behavior of activation energy, we slightly modified the energy states diagram, as suggested by J. Robertson.[35] The modified energy states diagram is presented in Fig. 10. Since tetrahedral amorphous carbon (taC), taC:H, and a-C:H act as weakly p-type, hence, we sketched Fermi level slightly below the mid-gap. The disorder semiconductors contain localized states near the Fermi level as well as in the band tail (lying slightly above and below the Fermi level). In addition, they also retain extended states. Hence, possible conduction in these semiconductors occur either through states near the Fermi level and states in the band tail or
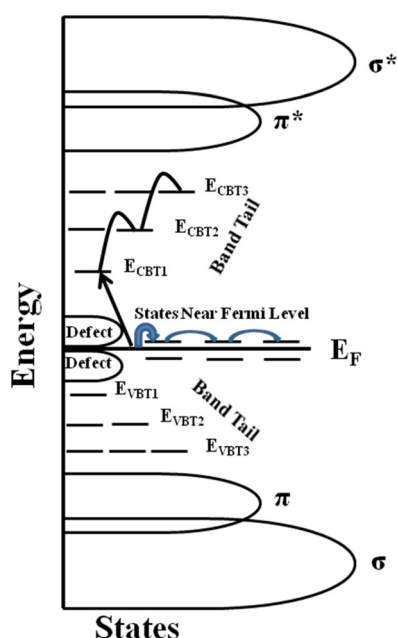
through extended states. The localized and defect states, which lie very near the Fermi level, are represented by states near the Fermi level and defect, respectively, in the schematic. In addition, the E_{CBT1}, E_{CBT2}, E_{CBT3}, etc. are the localized states in the band tail toward the conduction band side, whereas E_{VBT1}, E_{VBT2}, E_{VBT3}, etc. are the localized states in the band tail toward the valence band side. It is important to mention that states near the Fermi level as well as defect states are highly localized, whereas states in the band tail are weakly localized. In the low temperature range (300 K–363 K), where activation energy ΔE_{A1} was found to be extremely low, the conduction occurs in localized states at or near the Fermi level through phonon-assisted tunneling, as suggested in the model. However, at a higher temperature range (363 K–473 K), conduction happens through the localized states lying in the band tails. Each time, electrons jump from one localized state to another and exchange energy with the phonon. It is to be noted that states in the band tail are separated by comparatively larger energy gaps than states near the Fermi level. In the schematic, we presented, at higher temperature range (~363 K–473 K), that initially, an electron moves from the Fermi level to E_{CBT1}, then it moves from E_{CBT1} to E_{CBT2}, and this process continues until complete conduction. Silva et al.[36] have also obtained low activation energy in the temperature range 313 K–373 K and comparatively higher in the range 373 K–473 K. In addition, they also obtain activation energy with a value considerably lower than half the bandgap of the film. Further, a-C:N:H films showed comparatively higher activation energy than a-C:H films, due to the fact that the introduction of nitrogen reduces the defect density, localized states near the Fermi level, and localized states in the band tail.[37] Hence, under this situation, the charge carrier needed comparatively more energy to reach any localized states for conduction. Furthermore, it can be seen from Figs. 8(a)–8(h) that conductivity in both a-C:H and a-C:N:H films was found to enhance with the increasing self bias. Actually, a-C:H films contain both sp^3 and sp^2 sites of carbon. In a four-fold, coordinated sp^3 site, each carbon atom makes proper bonding with their nearest neighbor carbon atoms, resulting in unavailability of free electrons for conduction. On the other hand, a three-fold, coordinated sp^2 site associated with π-π* bonding contains one free electron. These π-π* bonds lie near the Fermi level and, therefore, control the conduction and E_g (as discussed earlier) of a-C:H films. Observed lower conductivity in a-C:H films deposited at self bias of −30 V was due to their polymer-like character, because, at lower self bias, the dissociation rate of a hydrocarbon precursor was low and a high fraction of hydrogen may be present in the film. However, increase in self bias to −100 V may lead to reduction in hydrogen and, thus, comparatively better conductivity, due to the diamond-like structure, was observed. Obtained maximum conductivity at a self bias of −180 V may be attributed to the initiation of graphite-like bonding. However, conductivity in a-C:N:H films was found to be comparatively better than a-C:H films. The conductivity ratio at high temperature (473 K) between a-C:N:H and a-C:H films deposited at low self biases −25 V and −30 V, respectively, was $1.46 \left(\frac{\sigma_{a-C:N:H}}{\sigma_{a-C:H}} = 1.46 \right)$ which increases to $2.8 \left(\frac{\sigma_{a-C:N:H}}{\sigma_{a-C:H}} = 2.8 \right)$ for

FIG. 10. (Color online) Modified model of Ref. 38 for electronic states of a-C:H and a-C:N:H films.

both types of films deposited at -100 V. The most remarkable change in conductivity of a-C:N:H films was observed at and above the self bias of -300 V. The maximum conductivity as $\sim 1 \times 10^{-4}$ Ω^{-1} cm^{-1} at 473 K in the a-C:N:H film was observed at a self bias of -400 V. The addition of nitrogen in a-C:N:H enhances the sp^2 clusters and sometimes it shifts the Fermi level toward the conduction band and, hence, enhances the conductivity, whereas higher self bias (above -100 V–200 V) promotes the formation of sp^2 clusters and, therefore, increases the conductivity. However, at lower self biases, some of the nitrogen may replace the hydrogen and reduce some bandgap and enhance the conductivity. The conductivity of a-C:N:H films was correlated with sp^3/sp^2 ratios, as estimated by FTIR analysis, and it was found to increase with the decreasing sp^3/sp^2 ratios. Since conductivity directly depends on bandgap, hence, we have also discussed conductivity as a function of bandgap. The variation of conductivity with bandgap is depicted in Fig. 11. The conductivity gets reduced with the increasing bandgap in both a-C:H and a-C:N:H films. However, here, do not confuse that a-C:H and a-C:N:H films with bandgap 2.85 eV and 2.75 eV, respectively, showed comparatively lower conductivity than these films having bandgap 3.45 eV and 3.33 eV, respectively. Because a-C:H and a-C:N:H films with bandgap 2.85 eV and 2.75 eV were polymer-like in nature, with bandgap 3.45 eV and 3.33 eV, respectively, they were diamond-like in nature. Nevertheless, I-V characteristics were also recorded to understand the semiconducting behavior of these films.

E. Current-voltage (I-V) analysis

The sandwich structure containing metal dots of Al of diameter 1 mm on substrates as well as on films was used to obtain I-V characteristics of a-C:H/n-Si and a-C:N:H/p-Si heterojunction devices. Since, in the present study, the temperature-dependent conductivity measurement confirms the semiconducting behavior of a-C:H and a-C:N:H films, a-C:H films were grown on n-Si and a-C:N:H films were deposited on p-Si substrates to form a-C:H/n-Si and a-C:N:H/p-Si heterojunction diodes, respectively. We have successfully demonstrated the fabrication of a-C:H/Si heterojunction diodes previously.[9] The I-V characteristics of a-C:H and a-C:N:H films are shown in Figs. 12(a)–12(h), where I-V
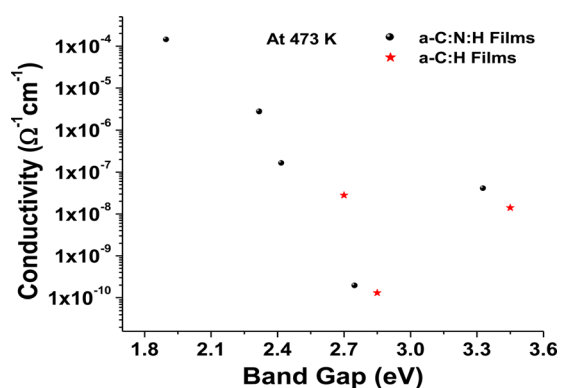
curves reveal the non-linear behavior and, therefore, the creation of rectifying circuits. Both types of structures, whether a-C:H/n-Si or a-C:N:H/p-Si, reveal one-way conduction. From Fig. 12(a)–12(c), it is evident that different a-C:H/n-Si heterojunction diodes turn on at different voltages, which is varied in between ~ 3 and ~ 4 V. In contrast, turn-on voltage in a-C:N:H/p-Si heterojunction diodes [Figs. 12(d)–12(h)] was varied in between ~ 2 V and 6 V. However, the magnitude of current in a-C:N:H/p-Si heterojunction diodes was found to be significantly more than a-C:H/n-Si heterojunction diodes, because addition of nitrogen in the a-C:N:H hetero-layer enhances the graphite-like sp^2 bonding. The a-C:H/n-Si heterojunction diodes showed a maximum value of current (at 10 V) of the order of $\sim 10^{-10}$ A, $\sim 10^{-9}$ A, and $\sim 10^{-7}$ A at the self biases of -30 V, -100 V, and -180 V, respectively. On the other hand, a-C:N:H/p-Si heterojunction diodes exhibited comparatively better magnitude of current (at 10 V) of the order of $\sim 10^{-9}$ A, $\sim 10^{-6}$ A, $\sim 10^{-3}$ A, $\sim 10^{-5}$ A, and $\sim 10^{-6}$ A at the self biases of -25 V, -100 V, -200 V, -300 V, and -400 V, respectively. In order to analyze electrical transport further, we plotted log I versus V characteristics for different a-C:H and a-C:N:H films and analyze the conduction mechanism in low and high voltages. The log I versus V plot reveals linear variation in the low voltage region that is accompanied by ohmic conduction and some bending of characteristics at the high voltage region. Thus, I-V characteristics were further fitted for Poole-Frankel and Schottky models. The variation of log I with V$^{1/2}$ for different a-C:H and a-C:N:H films is depicted in Figs. 13(a)–13(h). The investigation reveals that transport is bulk-limited, not ruled by differences at the barrier height at the contact. It is important to mention that, at higher voltages, the I versus V$^{1/2}$ plot shows straightening of the characteristic, which is the evidence of occurrence of the Poole-Frankel mechanism at higher voltages.

F. Nano-mechanical properties: a-C:N:H films as protective and encapsulate coating on solar cells

In order to explore a-C:N:H films as hard, protective, and encapsulate coatings on Si solar cells, particularly space solar cells, the transmission of films should be high and nano-mechanical properties, such as hardness (H), must be better. The nano-mechanical properties of a-C:N:H films were measured using the high resolution nanoindentation technique. Transmission analysis has already been done in Sec. III E, which reveals that a-C:N:H films have good optical transparency. The variation of H and elastic modulus (E) versus self bias for a-C:N:H films is shown in Figs. 14(a) and 14(b), respectively. Here, the value of H was initially increased with increasing self bias and attained maximum value at -100 V, beyond which it decreased continuously with the increasing self bias of -400 V. The values of H at -25 V, -100 V, -200 V, -300 V, and -400 V were found to be 8 GPa, 42 GPa, 29 GPa, 26 GPa, and 23 GPa, respectively. On comparing with Si, which shows H as ~ 11 GPa, the observed H in a-C:N:H films was found to be very high. Obtained maximum H at -100 V may be due to the creation of more sp^3 bonding, which is also confirmed by the maximum sp^3/sp^2 ratio at this

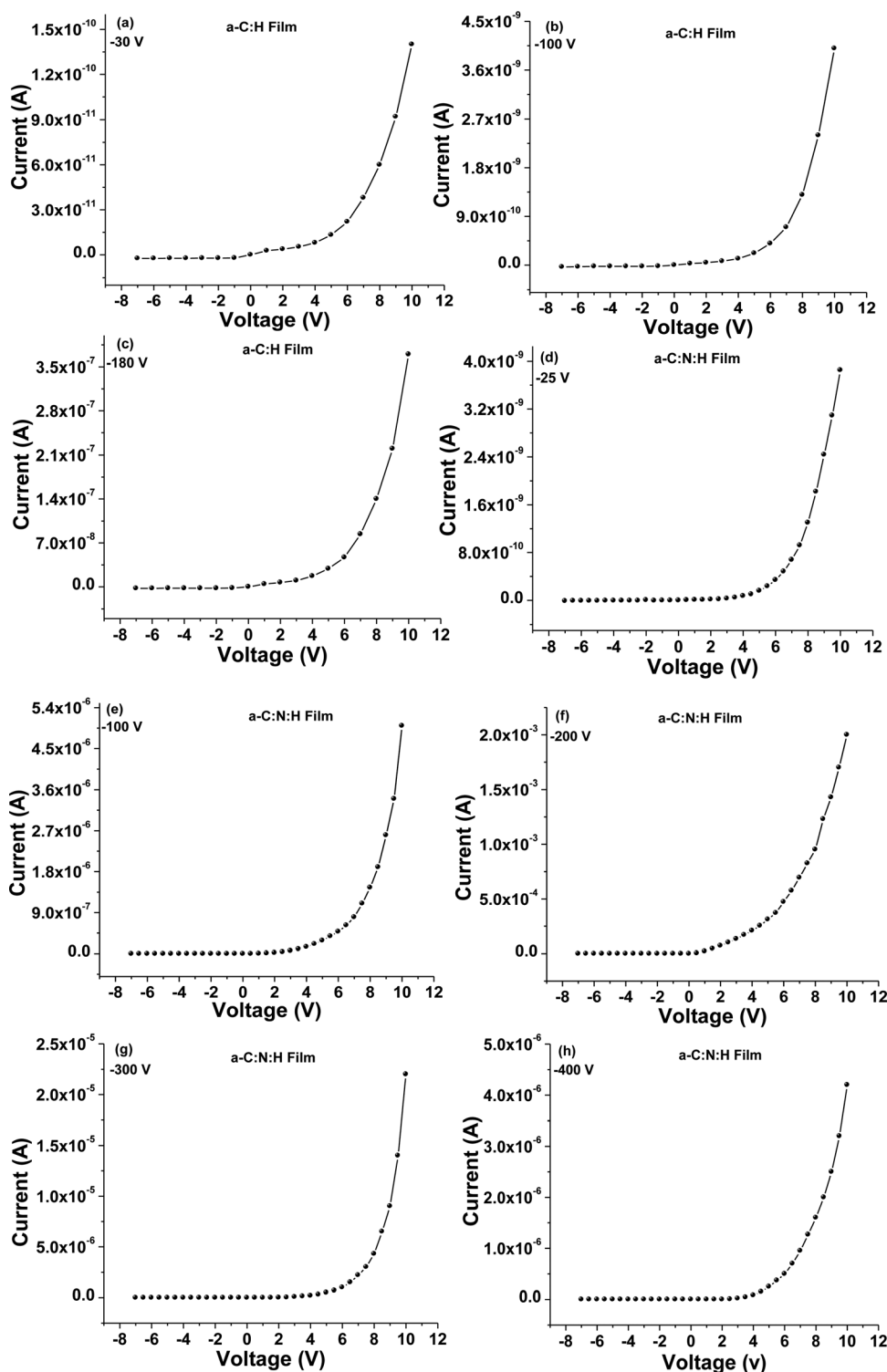FIG. 11. (Color online) Variation of conductivity with bandgap for different a-C:H and a-C:N:H films.

FIG. 12. (a)-(h) I-V characteristics of different a-C:H and a-C:N:H films.

self bias. An observed decrease in H beyond -100 V may be due to the initiation of graphite-like sp^2 bonding and, therefore, a decrease in sp^3/sp^2 ratios. However, minimum H at -25 V was due to the generation of polymer-like film. It is worth noting that a-C:N:H films showed high H and may withstand under the exposure of high energy radiation. Observed E results followed the similar trend and initially increased with increasing the self bias from -25 V to -100 V, beyond which it continuously decreased. The values of E at -25 V, -100 V, -200 V, -300 V, and -400 V were found to be 120 GPa, 430 GPa, 350 GPa, 330 GPa, and 302 GPa, respectively. Thus, a-C:N:H films can be used as hard, protective, and encapsulate coatings on Si solar cells.

IV. THEORETICAL ANALYSIS

A. Why variable bandgap layers for full spectrum solar cells?

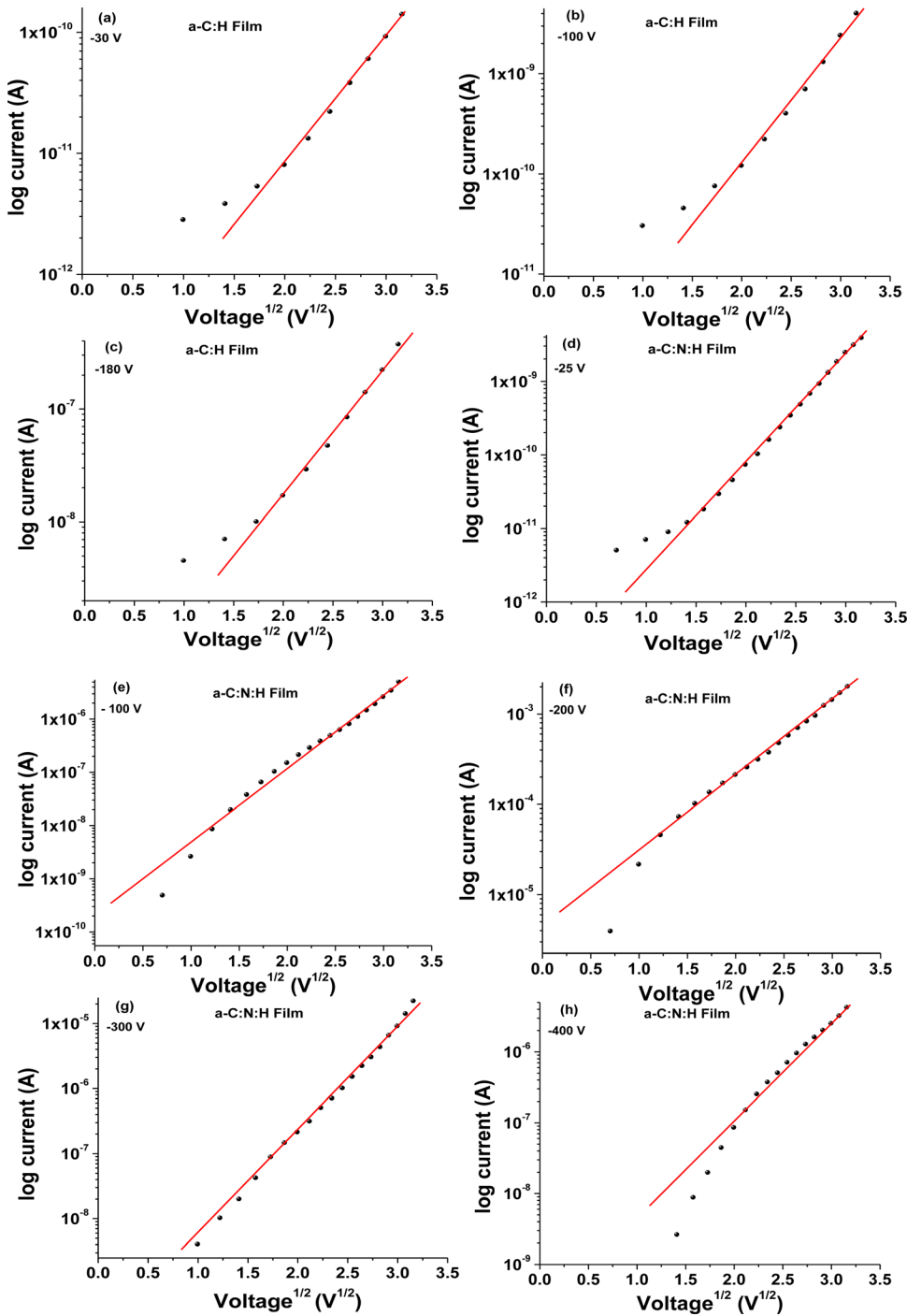When the light falls on the solar cells, then one of the following situations are possible

FIG. 13. (Color online) Poole-Frankel model (I vs $V^{1/2}$ characteristics) of different a-C:H and a-C:N:H films.

$$h\upsilon < E_g, \qquad (4)$$

$$h\upsilon > E_g \qquad (5)$$

$$h\upsilon = E_g, \qquad (6)$$

where $h\upsilon$ is the energy of photon and E_g is the optical bandgap of the material. In the first case, when $h\upsilon \leq E_g$, i.e., if the energies of photons are lower than the bandgap of the material, no generation of a photo-induced electron holes pair takes place and, hence, no contribution to efficiency. However, in the second case, when $h\upsilon \geq E_g$, i.e., if the energies of photons are higher than the bandgap of material, the

efficiency of the cell reduces, due to an increase in power dissipation (heat energy). In the third and last case, when $h\upsilon = E_g$, i.e., if the energies of photons match with the bandgap of the material, then the highest efficiency may be achieved. As a-Si:H is a widely used material for solar cell, but due to its fixed and lower bandgap, most of the light results into heat, therefore, lower efficiency is realized. There is no material that is sensitive to all wavelengths of the spectrum. In order to make such a material that could respond full-spectrum, the material must have bandgap feasibility over a wide range. This type of full-spectrum solar cell can be useful to improve the efficiency of a cell significantly. This is the reason why the research on full-spectrum solar
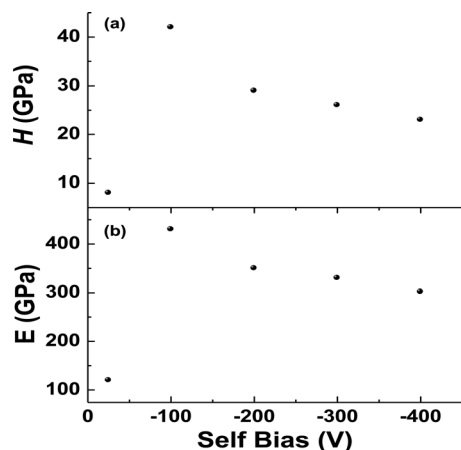
FIG. 14. Variation of H and E with self bias for a-C:N:H films.

cells is at a peak in the present time. Lopez et al.[38] have worked significantly for the development of a practical full-spectrum solar cell. Such full-spectrum solar cells are possible when a number of varied bandgap layers stack on one another in a proper manner. The multijunction solar cells, which are also referred to as tandem solar cells, can be another approach toward full-spectrum solar cells. In the present study, we have grown varied bandgap layers of a-C:H and a-C:N:H films by nitrogen incorporation and tuning of self bias. The bandgap in these films was varied from 1.9 eV to 3.45 eV, which covered almost an entire visible range ($\sim$1.7 eV to $\sim$3.3 eV). Further, by optimizing process parameters, the lower bandgap region, i.e., 1 eV to 1.9 eV, may also be possible. Recently, we deposited oxygen-modified DLC films with varied bandgap in the range 1.25 eV–2.6 eV.[30] So, this may cover an almost full-spectrum from $\sim$1 eV to $\sim$3.5 eV, and an efficient solar cell may be experimentally realized.

B. Proposed multilayer and multijunction structure for full-spectrum solar cells

We have observed variable bandgap layers, in which the bandgap varies from 1.9 eV to 3.45 eV. Thus, with these layers, we may have two different structures, namely, multilayer and multijunction structure, for full-spectrum solar cells. Tinchev et al.[11] have recently discussed the DLC-based multilayer structure to respond for wide solar spectrum. We propose the usefulness of varied bandgap multilayer structure for solar cells. Figure 15(a) shows the designing of different bandgap layers regarding their response for full solar spectrum. In the schematic, the high bandgap window layer w_1-a-C:H was kept at the top and the remaining a-C:H and nitrogen-modified a-C:N:H window layers were kept in decreasing bandgap order. However, i and n layers of a-Si:H with bandgap $\sim$1.75 eV were kept in the bottom. On exposing the solar spectrum ($\sim$350 nm to 1240 nm) on this structure, first, the w_1-a-C:H layer with bandgap 3.45 eV will absorb spectrum below 360 nm and the rest of the radiation will be transmitted to the next layer. The next w_2-a-C:H layer, with bandgap 2.7 eV, will absorb the light in between 360 and 460 nm as well as some fraction of light in the range of 350 nm and 360 nm if the first layer does not absorb the entire light of this range. It is important to mention that, due to the interface of the first and second window layers, some of the light may also be reflected. The third nitrogen-modified w_3-a-C:N:H layer, with bandgap 2.32 eV, will absorb the light below 535 nm and, above this wavelength, the light will be transmitted to the next layers. In contrast to the interface of the first and second layers, the absorbance loss in the interface between the second and third layers will be negligible, because some reflected light may be absorbed in different layers. Similarly, the fourth w_4-a-C:N:H layer, with bandgap 1.9 eV, will absorb light below 653 nm and the rest of the light will be transmitted to the
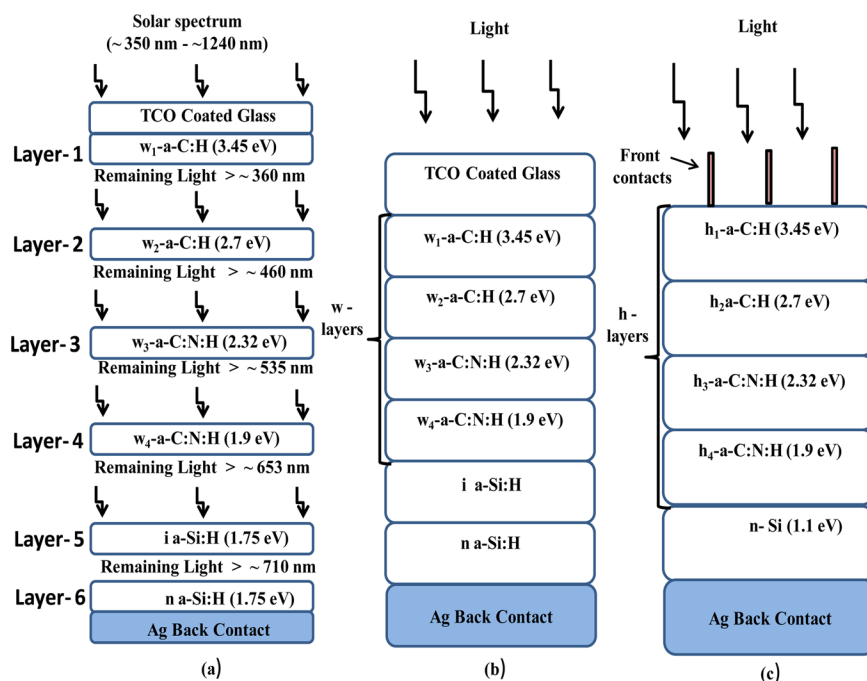

FIG. 15. (Color online) (a) and (b) The proposed aSi:H-based thin film solar cell structure, where variable bandgap a-C:H and a-C:N:H multilayer are considered as window (w) layer and (c) proposed carbon/silicon heterojunction solar cell, where a-C:H and a-C:N:H multilayers are used as heterolayer.

a-Si:H layers. The absorption loss due to interfaces will be decreased with the distance deep into the structure. So, in this layer, the absorption loss due to the interfaces will be negligible. Further, the remaining solar spectrum will be transmitted to the a-Si:H i layer with bandgap ∼1.75 eV that will absorb the light below 710 nm. Thus, with this design, we may cover the entire visible region and move toward the full spectrum solar cell (∼1 eV to ∼3.5 eV) by the multilayer concept. Figure 15(b) shows the simplified design of such a multilayer solar cell, where different a-C:H and nitrogen-modified a-C:N:H layers were considered as window layers that have p-type property. It is important to mention that, while preparing multilayer solar cells, the thickness and the interface are found to be a big issue and must be optimized properly. Instead of a p-i-n device, if we grow variable bandgap a-C:H and a-C:N:H heterolayers on a Si wafer, the full-spectrum heterostructure solar cell is possible. Hence, we propose another design to produce near full-spectrum solar cells by a multilayer DLC/silicon-based heterostructure approach. The proposed design of such a structure is depicted in Fig. 15(c). In this design, the a-C:H and a-C:N:H heterolayers will be deposited on a Si wafer with a bandgap of 1.1 eV. On shining the light on multilayer DLC/silicon heterostructure, the top four a-C:H and a-C:N:H heterolayers (from h_1 to h_4) will absorb the light below ∼653 nm and rest of the light will go to the wafer. The n-type Si wafer with a bandgap of 1.1 eV will also absorb the light below ∼1127 nm. Thus, with this design, an almost entire solar spectrum may be covered, and it may be a novel approach to move toward full-spectrum solar cells. We again emphasize that the thickness and interface of a-C:H and a-C:N:H multilayers for heterojunction must be optimized properly. We have also experimentally prepared the carbon/silicon-based hetero-junctions earlier.[9]

Besides multilayer, the tandem solar cells may also be another approach to design the full-spectrum solar cells. We propose three and four junctions tandem solar cells, where different a-C:H and a-C:N:H layers are considered as window layers. Figure 16(a) and 16(b) show the three and four junctions tandem solar cells with a-C:H- and a-C:N:H-based w_1, w_2, w_3, and w_4 as window layers. With these tandem configurations, hard, efficient, durable, and cost-effective solar cells may be realized. Recently, Kabir et al.,[5] also proposed high efficiency double and triple junction solar cells with wide bandgap p-layers. These a-C:H and a-C:N:H films may also be used as a window layer in a-Si:H-based single junction p-i-n solar cells. Khan et al.,[39] Lee et al.,[7] and Tian et al.[40] have generated an a-Si:H p-i-n solar cell, taking amorphous carbon as the p-type window layer. Hence, we have also performed the simulation study for a-Si:H-based thin film solar cells, where a-C:H and a-C:N:H films were considered as window layers.

C. Simulation study

The schematic of proposed single junction a-Si:H thin film solar cells with a-C:H and a-C:N:H as window layers are depicted in Fig. 17. Since we have grown eight different bandgap a-C:H and a-C:N:H layers, eight solar cell designs
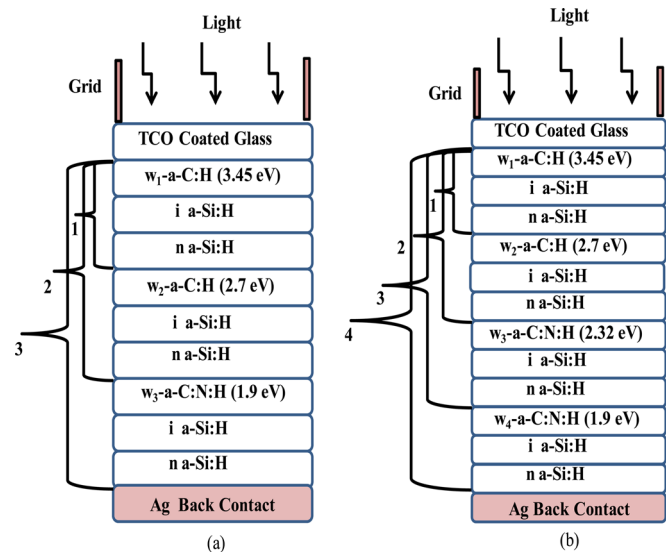

FIG. 16. (Color online) (a) Proposed a-Si:H-based multijunction solar cell having junction (a) three and (b) four and with a-C:H and a-C:N:H as window layers.

are possible. Hence, simulation was performed by varying window layer band gaps from 1.8 eV to 3.45 eV, which also included these experimentally realized band gaps. The standard values of different parameters for i and n a-Si:H layers as well as a-C:H and a-C:N:H window layers were considered for simulation, which are shown in Table I. Figure 18(a) shows the variation of efficiency with bandgap of a-C:H and a-C:N:H window layers. Besides the efficiency, various other important parameters, such as open circuit voltage (V_{oc}), short circuit current density (J_{sc}), and fill factor (FF), were also evaluated. V_{oc} was reduced from ∼1324 mV to ∼1301 mV and J_{sc} was enhanced from ∼10.95 mA/cm^2 to ∼13 mA/cm^2 with the increasing bandgap from 1.8 eV to 3.45 eV. The increased current density with the increasing bandgap was due to the fact that most of the light transmitted to the i-layer, where it gets absorbed and enhances the population of electron-hole pairs. Since the fill factor (FF) varies inversely with the V_{oc}-J_{sc} product and with the increasing bandgap, J_{sc} was enhanced, but V_{oc} was reduced significantly; FF was drastically enhanced from ∼21.3% to ∼84.1%, with the increasing bandgap from 1.8 eV to 3.45 eV. Further, depending upon their variation with bandgap, efficiency was divided into three regions (R-I to R-III), which is shown in Fig. 18(a). In the beginning bandgap from 1.8 eV to 2.1 eV (R-I), the efficiency (at window layer 5 nm) was enhanced gradually and it slightly falls in the range 2 eV to 2.1 eV. However, beyond 2.1 eV up to 3.15 eV (R-II), efficiency (at window layer thickness 5 nm) gets continuously enhanced with the increasing bandgap.

Beyond 3.15 eV up to 3.45 eV (R-III), the efficiency (at window layer thickness 5 nm) gets saturated. The highest efficiency as 14.2% (at window layer thickness 5 nm) was observed in the range 3.2 eV to 3.45 eV. The efficiency gets reduced with the increasing window layer thickness from 5 nm to 20 nm in all the regions from R-I to R-III. Observed low efficiency in the low bandgap region (R-I) may be due to holes trapping at the p-i interface and flattening of the
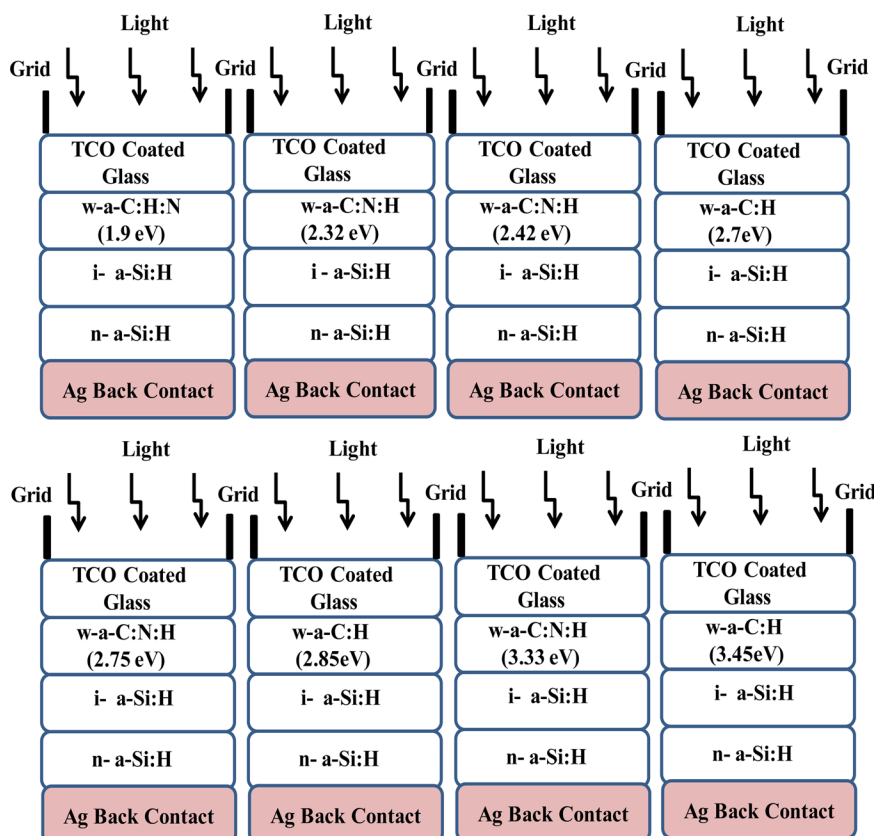
FIG. 17. (Color online) Proposed a-Si:H-based single junction thin film solar cell, where a-C:H and a-C:N:H are used as window layers.

band over the i-layer. However, if thickness is considered (window layer thickness greater than 5 nm), besides trapping of holes and the flattening of the band, high absorption losses were also found to be a cause of lower efficiency in low bandgap. Nonetheless, with the increasing bandgap from
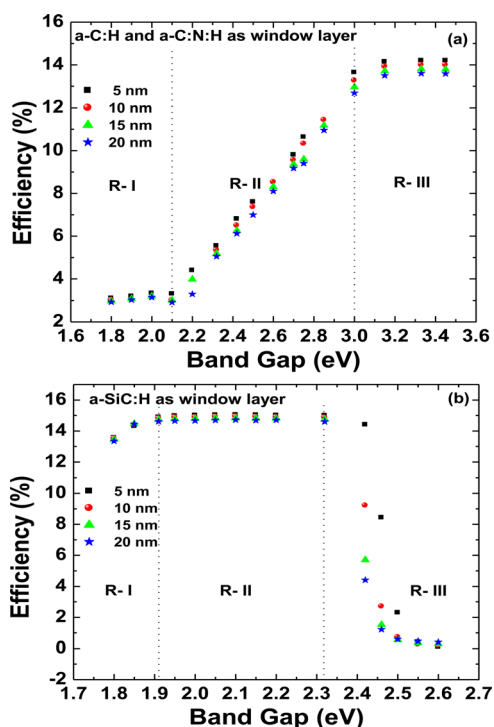

FIG. 18. (Color online) Variation of computer-simulated efficiency of single junction a-Si:H thin film solar cell with (a) window layer bandgap of a-C:H and a-C:N:H and (b) window layer bandgap of a-SiC:H.

2.1 eV to 3.15 eV (R-II), the absorption losses and the flattening of band over the i-layer was reduced and the hole trapping at the w-i interface may be relaxed and, hence, high efficiency was realized. However, with the increasing window layer bandgap from beyond 3.15 eV up to 3.45 eV (R-III), the efficiency remains almost stable, due to an optimum of the input parameters. Hence, by considering a-C:H and a-C:N:H as window layers in a-Si:H thin film solar cells, the maximum efficiency as 14.2% at a higher bandgap was realized.

Since a-SiC:H is a conventional, wide-bandgap window layer for a-Si:H thin film solar cells, simulation by considering a-SiC:H as a window layer was also performed and obtained results were compared with the previous one. Variation of efficiency with the bandgap of the a-SiC:H window layer is depicted in Fig. 18(b). Similar to the a-C:H and a-C:N:H window layer, the variation of efficiency with bandgap for the a-SiC:H window layer was also divided into three regions (R-I, R-II, and R-III). With the increasing a-SiC:H window layer bandgap from 1.8 eV to 1.91 eV (R-I), efficiency was enhanced gradually and became constant beyond 1.91 eV up to 2.32 eV (R-II). The value of efficiency was found to be ~15% in the range 1.95 eV–2.32 eV. On further enhancement of the bandgap from 2.32 eV to 2.5 eV (R-III), efficiency fell sharply and became negligible beyond 2.5 eV. In addition, with the increase of thickness of the window layer, efficiency was reduced in each bandgap. It is important to mention that, in the bandgap range of 2.32 eV–2.5 eV, thickness had a pronounced effect on the efficiency of the solar cell. Further, although efficiency by considering a-C:H and a-C:N:H as the window layer was found to be slightly lower (14.2% in the range 3.2 eV–3.45 eV) than in the case of a-SiC:H as the window layer (15% in the

range 1.95 eV–2.35 eV), this a-C:H and a-C:N:H can be a better window layer, owing to the following other aspects:

(a) Fabrication of a-SiC:H is quite more complicated than a-C:H and a-C:N:H films
(b) Fabrication of a-SiC:H also requires silane, which is a highly flammable gas
(c) Compared with a-C:H and a-C:N:H, a-SiC:H is expensive
(d) Discrepancy during growth of a thin a-SiC:H layer, due to the employment of two gases, like silane and methane or acetylene
(e) Similar to a-C:H and a-C:N:H, a-SiC:H is also harder, but its mechanical properties may be degraded in case of improper stoichiometry
(f) Compared with a-SiC:H, high hardness and wear resistance made a-C:H and a-C:N:H window layers suitable for space solar applications, as space vehicles face high energy radiation, including Gamma radiation, solar wind, etc.
(g) Limitation in bandgap feasibility and, hence, the utilization of only certain solar spectrum in the case of a-SiC:H as the window layer is realized. In contrast, with a-C:H and a-C:N:H as the window layer, covering of the full solar spectrum is possible.
(h) The last and most important fact is that a-C:H and a-C:N:H window layers can be deployed in an a-Si:H-based multijunction and tandem solar cells easily, due to wide bandgap flexibility, and very high efficiency can be obtained

V. POSSIBLE APPLICATIONS

Due to experimentally estimated fascinating electrical, optical, and nano-mechanical properties, these a-C:H and a-C:N:H films may find wide industrial application. In the present work, we demonstrated the formation of a-C:H or a-C:N:H/silicon heterojunction as well as semiconducting behavior of various a-C:H and a-C:N:H films. In addition, we performed simulation studies, considering a-C:H as the window layer. Hence, it is expected that these films can be used in the development of an efficient amorphous silicon solar cell. Moreover, excellent nano-mechanical properties with hardness close to 42 GPa can leads to their uses as hard and protective coating on cutting tools and automobile parts as well as on silicon solar cells. In addition, use of a-C:H and a-C:N:H as the window layer, particularly in the n-i-p configuration on metal substrate, can minimize additional hard and protective coating and, hence, reduce the cost of the product, which can be effectively used for space solar cell applications.

VI. CONCLUSIONS

We have used asymmetric, capacitive–coupled RF-PECVD technique for the deposition of a-C:H and a-C:N:H films under varied self bias. The electrical, optical, and nano-mechanical properties were studied in order to explore these films as materials for solar cell application. The incorporation of nitrogen and increase in self bias decreased the residual stress of a-C:H and a-C:N:H films significantly. The introduction of nitrogen and an increase in self bias also improved the electrical properties and tuned the bandgap over a wide range. I-V characteristics exhibited one-way conduction (rectifying behavior) and confirmed the hetero-junction formation. The tuning of the bandgap over a wide range may lead these films to their application for fabrication of multilayer and tandem solar cells. We also proposed multilayer and tandem solar cells by considering variation of bandgap of these layers. Such wide bandgap a-C:H and a-C:N:H films may also act as heterolayers to form heterojunctions with a Si wafer. We also performed simulation studies and observed that the use of a-C:H and a-C:N:H enhances the efficiency of solar cells significantly. In addition, a-C:N:H films exhibited improved nano-mechanical properties that may lead them to their use as protective and encapsulate coating on solar cells. In conclusion, a-C:H and a-C:N:H films, in various ways, can be used to improve the efficiency of existing a-Si:H-based solar cells.

[1]K. L. Chopra, P. D. Paulson, and V. Dutta, Prog. Photovoltaics **12**, 69 (2004).
[2]N. Palit and P. Chatterjee, J. Appl. Phys. **86**, 6879 (1999).
[3]J. K. Rath and R. E. I. Schropp, Sol. Energy Mater. Sol. Cells **53**, 189 (1998).
[4]A. S. Ferlauto, G. M. Ferreira, J. M. Pearce, C. R. Wronski, R. W. Collins, X. Deng, and G. Ganguly, J. Appl. Phys. **92**, 2424 (2002).
[5]M. I. Kabir, Z. Ibrahim, K. Sopian, and N. Amin, Sol. Energy Mater. Sol. Cells **94**, 1542 (2010).
[6]K. M. Krishna, M. Umeno, Y. Nukaya, T. Soga, and T. Jimbo, Appl. Phys. Lett. **77**, 1472 (2000).
[7]C. H. Lee and K. S. Lim, Appl. Phys. Lett. **75**, 569 (1999).
[8]J. F. Lee, Z. Y. Yang, and R. F. Xiao, J. Appl. Phys. **80**, 5398 (1996).
[9]S. Kumar, N. Dwivedi, C. M. S. Rauthan, and O. S. Panwar, Vacuum **82**, 882 (2010).
[10]N. Dwivedi, S. Kumar, C. M. S. Rauthan, and O. S. Panwar, Plasma Processes Polym. **8**, 100 (2011).
[11]S. S. Tinchev, P. I. Nikolova, J. T. Dyulgerska, G. Danev, and T. Babeva, Sol. Energy Mater. Sol. Cells **86**, 421 (2005).
[12]V. G. Litovchenko and N. I. Klyui, Sol. Energy Mater. Sol. Cells **68**, 55 (2001).
[13]N. Dwivedi, S. Kumar, C. M. S. Rauthan, and O. S. Panwar, Appl. Phys. A **102**, 225 (2011).
[14]N. Dwivedi, S. Kumar, R. K. Tripathi, H. K. Malik, and O. S. Panwar, Appl. Phys. A **105**, 417 (2011).
[15]N. Dwivedi, S. Kumar, H. K. Malik, Govind, C. M. S. Rauthan, and O. S. Panwar, Appl. Surf. Sci. **257**, 6804 (2011).
[16]N. Dwivedi, S. Kumar, Ishpal, S. Dayal, Govind, C. M. S. Rauthan, O. S. Panwar, J. Alloys Compd. **509**, 1285 (2011).
[17]N. Dwivedi and S. Kumar, Curr. Appl. Phys. **12**, 247 (2012).
[18]V. A. Dao, J. Heo, H. Choi, Y. Kim, S. Park, S. Jung, N. Lakshminarayan, and J. Yi, Sol. Energy **84**, 777 (2010).
[19]P. Mahtani, K. R. Leong, I. Xiao, A. Chutinan, N. P. Kherani, and S. Zukotynski, Sol. Energy Mater. Sol. Cells **95**, 1630 (2011).
[20]W. I. Milne, Semicond. Sci. Technol. **18**, 81 (2003).
[21]J. Robertson, Diamond Relat. Mater. **5**, 797 (1996).

[22]Z. Yu, I. Pereyra, and M. N. P. Carreno, Sol. Energy Mater. Sol. Cells **66**, 155 (2001).

[23]L. Zhao, C. L. Zhou, H. L. Li, H. W. Diao, and W. J. Wang, Sol. Energy Mater. Sol. Cells **92**, 673 (2008).

[24]L. Zhao, H. L. Li, C. L. Zhou, H. W. Diao, and W. J. Wang, Sol. Energy **83**, 812 (2009).

[25]S. V. Singh, T. Zaharia, M. Creatore, R. Groenen, K. V. Hege, and M. C. M. van de Sanden, J. Appl. Phys. **107**, 013305 (2010).

[26]J. T. Titantah, D. Lamoen, E. Neyts, and A. Bogaerts, J. Phys.: Condens. Matter **18**, 10803 (2006).

[27]J. K. Walters, R. J. Newport, S. F. Parker, W. S. Howells, and G. Bushnell-Wye, J. Phys.: Condens. Matter **10**, 4161 (1998).

[28]F. L. Freire, J. Non-Cryst. Solids **304**, 251 (2002).

[29]J. Robertson, Semicond. Sci. Technol. **18**, 12 (2003).

[30]N. Dwivedi, S. Kumar, S. Singh, and H. K. Malik, Sol. Energy **86**, 220 (2012).

[31]M. Sharon, S. Jain, P. D. Kichambare, and M. Kumar, Mater. Chem. Phys. **56**, 284 (1998).

[32]M. Sharon, I. Mukhopadhyay, and K. Mukhopadhyay, Sol. Energy Mater. Sol. Cells **45**, 35 (1997).

[33]K. Mukhopadhyay, I. Mukhopadhyay, M. Sharon, T. Soga, and M. Umeno, Carbon **35**, 863 (1997).

[34]K. M. Krishna, T. Soga, K. Mukhopadhyay, M. Sharon, and M. Umeno, Sol. Energy Mater. Sol. Cells **48**, 25 (1997).

[35]J. Robertson, Philos. Mag. B **76**, 335 (1997).

[36]S. R. P. Silva, J. Robertson, G. A. J. Amaratunga, B. Rafferty, L. M. Brown, J. Schwan, and G. Marriotto, J. Appl. Phys. **81**, 2626 (1997).

[37]C. Godet, N. M. J. Conway, J. E. Bouree, K. Bouamra, A. Grosman, and C. Ortega, J. Appl. Phys. **91**, 4154 (2002).

[38]N. Lopez, L. A. Reichertz, K. M. Yu, K. Campman, and W. Walukiewicz, Phys. Rev. Lett. **106**, 028701 (2011).

[39]R. U. A. Khan, S. R. P. Silva, and R. A. C. M. M. van Swaij, Appl. Phys. Lett. **82**, 3979 (2003).

[40]X. M. Tian, M. Rusup, Y. Hayashi, T. Soga, T. Jimbo, and M. Umeno, Sol. Energy Mater. Sol. Cells **77**, 105 (2003).